Identification of Adipogenic and Osteogenic Differentiation using transfer learning of ResNet-18

Maxwell Mai
Department of Mathematics
Southern Connecticut State University
New Haven, Connecticut, USA

Shuai Luo
Department of Chemistry, Chemical and Biomedical Engineering
University of New Haven
West Haven, Connecticut, USA

Shue Wang
Department of Chemistry, Chemical and Biomedical Engineering
University of New Haven
West Haven, Connecticut, USA
Email: swang@newhaven.edu

Yulei Pang
Department of Mathematics
Southern Connecticut State University
New Haven, Connecticut, USA
Email: pangy1@southernct.edu

2023 International Conference on Machine Learning and Applications (ICMLA) | 979-8-3503-4534-6/23/$31.00 ©2023 IEEE | DOI: 10.1109/ICMLA58977.2023.00135

***Abstract*—Human mesenchymal stem cells (hMSCs) have great potential in cell-based therapies and regenerative medicine due to their self-renewal and multipotency. hMSCs can be differentiated into several cell types, including adipocytes and osteblast. Conventional approaches for determining adipocyte formation include staining of lipid droplets (i.e., oil-red-O) during adipogenesis, which is time-consuming and uneconomical. Thus, there is an emerging need for a more effective and accurate approach to the prediction of adipogenic differentiation. Here, by combining live-cell imaging with a deep learning method, we developed a convolutional neural network-based approach to precisely predict lipid droplet formation during adipogenic differentiation of hMSCs.**

***Index Terms*—Transfer learning, Deep learning, CNN, hMSCs, Adipogenic differentiation, ResNet, convolution, computer vision, osteogenic differentiation, human mesenchymal stem cells, adipogenisis**

I. INTRODUCTION

Mesenchymal stem cells (MSCs) have great potential for tissue engineering, regenerative medicine, and cell-based therapies due to their capacity of self-renewal and multi-potency. Under certain chemical or biophysical stimulations, MSCs can be differentiated into various lineages, including osteoblasts, adipocytes, neurons, and chondrocytes [1]. Although MSCs hold great potential for both regenerative medicine and novel therapeutic discovery, MSC based clinical trials are currently limited due to inconsistent therapeutic affects, including functional heterogeneities among different donors, stemness stability, differentiation capacity, and variation in MSCs production [2]. Thus, an automated, robust approach for identifying differentiation is required for effective quality control of MSCs functions. Recently, it has been reported that MSCs functions, particularly differentiation potential, relate to cell morphology [3], [4], [5]. For example, MSCs morphology has been correlated with differentiation capacity [6], [7], [8] and passage number [9]. Recent advancements in machine learning provide the opportunity for predicting a stem cell's fate by utilizing large data sets of stem cell characteristics [10], [11], [12]. Among these machine learning methods, deep learning techniques have emerged as powerful tools to predict and identify stem cell patterns and lineage relationships [13]. Machine learning algorithms have been used to predict MSC osteogenic potential [6], [7], micro-environmental cues, neural stem cell differentiation, and blastocyst formation [10]. However, the majority of the machine learning-based approaches are built on data collected from fixed cells through immunoflourescent (IF) staining, which is more time consuming and expensive than stainless live cell imaging. Thus, there is an urgent need for an effective deep learning-based approach that can accurately predict and identify the fate of stem cells without causing cell fixation or requiring staining. To advance this field, we aim to investigate whether a morphology-based prediction model, using a data set obtained through stainless live cell imaging is capable of predicting adipogenic and osteogenic differentiation in cells. Adipogenic differentiation, the process of mature fat cell formation, plays a crucial role in adipose tissue development and metabolic regulation. Accurate prediction and identification of cells undergoing adipogenic differentiation can provide valuable insights into various physiological and pathological conditions. In this study, we aim to develop an efficient and robust tool for identifying adipogenic differentiated cells based on cellular morphology by leveraging the power of deep learning and image analysis. The model will be trained on a dataset of labelled cell images and will learn to capture key morphological features associated with adipocyte and osteocyte formation. In this study we will show that the ResNet 18 for transfer learning can classify images with slight morphological variations correctly, with satisfactory results on Accuracy, Precision, Recall. Our research aims to assess the effectiveness of ResNet architectures for adipocyte identification on images of hMSCs. Our findings reveal that ResNet can accurately identify stem cell patterns with a high degree of stability, all while requiring a relatively small number of labelled training examples.

The rest of the paper is organized as follows.

1946-0759/23/$31.00 ©2023 IEEE
DOI 10.1109/ICMLA58977.2023.00135

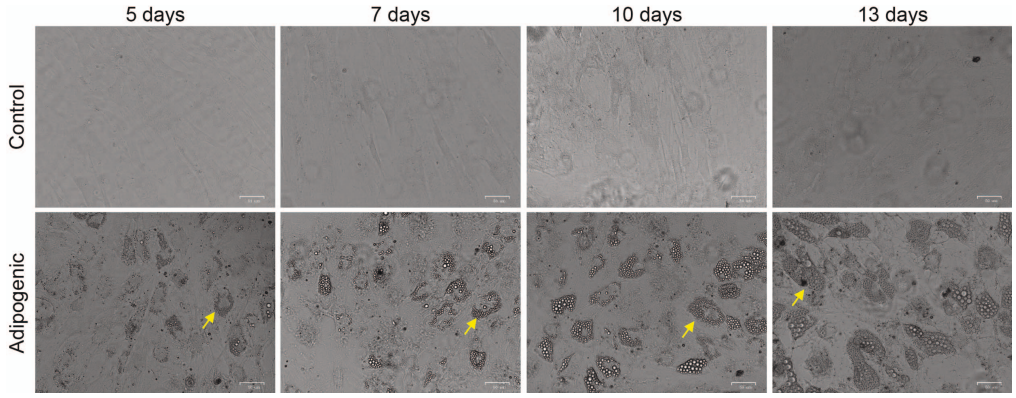

Fig. 1. Bright field images of hMSCs under control and adipogenic differentiation conditions at different time points, Scale bar: 50 μm

- Section II, presents the description of the dataset, pre-processing methods, models, and statistical analysis done in this study. A detailed background of image collections, training details, hyper parameter tuning, and architecture of our customized ResNet model are presented.
- Section III, explains how the experiments are performed and presents the evaluation of customized ResNet18 model.
- Section IV, concludes the paper, presents the limitations of the study and the conclusion and gives perspectives for future work.

II. MATERIALS AND METHODS

A. Cell Culture and Reagents

Our Human mesenchymal stem cells (hMSCs) were acquired from Lonza. According to the manufacture, hMSCs were isolated from normal (non-diabetic) adult human bone marrow withdrawn from bilateral punctures of the posterior iliac crests of normal volunteers. hMSCs were maintained in mesenchymal stem cell basal medium with GA-1000, L-glutamine, and mesenchymal cell growth supplements. The cells were cultured in a humidified incubator at 37 °C with 5 percent CO_2 and passaged using 0.25 Trypsin-EDTA (Invitrogen). The cell culture medium was replaced every three days. hMSCs from passages 3-7 were used in the experiments.

To induce adipogenic differentiation, hMSCs were seeded at a density of 1x 104 cells/mL with a volume of 700 μL in 12 well-plates. When cells reach 80-90 percent confluency, the basal medium was replaced with adipogenic induction medium, which is supplemented with induction and growth factors. Adipogenic induction medium was changed every three days. Images were taken after 5 days, 7 days, 10 days and 13 days of induction, respectively.

B. Characteristics of hMSCs

Mesenchymal stem cells have the capability to differentiate into various cell types including adipocytes through adipogenic induction. The adipogenic differentiation of hMSCs can be characterized by intracellular accumulation of lipid droplets as well as specific adipocyte transcription genes, for example, PRAR- γ. The adipogenic differentiation process includes four stages, growth arrest, mitotic clonal expansion (MCE), early differentiation, and late differentiation. Fig. 1 shows bright field images of hMSCs under control and adipogenic induction conditions. In the control group, hMSCs were cultured with the basal medium. As shown in the upper panel of Fig. 1 , hMSCs display a spinal shape without chemical induction. After adipogenic induction, hMSCs went through growth arrest, clonal expansion (5 days), and early differentiation (7, 10, and 13 days). Under adipogenic differentiation, hMSCs morphology changes, and cells accumulate lipid droplets internally. As the adipocyte matures, the amount of lipids increases until almost the entire cell volume is occupied, as indicated in the yellow arrow.

C. Related work

Several seminal works have laid the foundation for machine learning based methodology to identify cell differentiation.

In 2013 Matsuoka et al. [14] has applied Ridge Regression as the machine learning modeling method to quantitatively predict cellular osteogenic potential.

Support Vector Machine algorithm and "supercell" clustering of single cells was used to identify the cell morphology features which best describe hBMSC population cell morphology. alterations associated with the transition (NF1 to NF2) of hBMSC osteogenic differentiation modulated by nanofiber densities [15], [16].

A transfer learning-based approach was utilized as the feature extractor by Kim et al. (2022) [17], with four well-performing models (VGG19, InceptionV335, Xception, and DenseNet121) pre-trained on ImageNet. With over 85% accuracy, the results demonstrated the potential of a computer vision based method for identifying stem cell differentiation.

More recently, Zhou et al. (2023) [18] introduced a predictive model for classifying hMSC differentiation lineages using the k-nearest neighbors (kNN) algorithm. It provided accurate prediction of lineage fate on different types of biomaterials as early as the first week of hMSCs culture with an overall accuracy of 90.63% on the test data set.

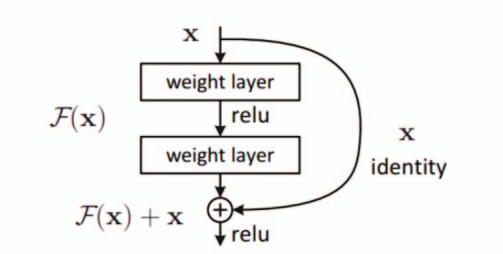

Fig. 2. A Basic Residual Block

III. Model

A. Transfer Learning

Transfer learning is defined as applying a model trained on a general task to a new related task ([19]). Building a model using only cell images as training data is often not the most practical strategy since it requires large computational resources, and high quality labeled data is scarce. In addition, the deeper a network becomes (i.e. the more layers it has), the more training data it requires to converge on a best estimate for all parameters. Pre-trained convolutional neural networks (CNNs) have been trained on large-scale data sets and have learned general feature representations that capture meaningful patterns and structures in images of all types. In order to properly adapt these models to our task, we provide additional training data that is used to fine tune the parameters of the final layers in the network. [20].

B. ResNet Architectures

The deep residual network (ResNet) is one of the most common convolutional neural networks (CNN), developed by He et al [21]. The residual building block (RBB) is the most vital element in ResNet18. The RBB is based on the idea of skipping blocks of convolution layers by using shortcut connections (see Fig. 2). These shortcuts are useful to avoid the vanishing/exploding gradients problem, which helps us to construct deeper networks and improves final performance for fault diagnosis [22]. In other words, since convolution is a lossy process, short cutting inputs and recombining them with their convoluted outputs allows for a better flow of gradient information in very deep networks.

Each image in our data set has a high number of dimensions, 2592 x 1944 pixels, and much of the space is essentially empty. To reduce the dimensionality of the images, and eliminate unnecessary information we employ a convolutional neural network, specifically ResNet 18 [21].

This architecture consists of seventeen convolution layers followed by an average pooling layer and two fully connected layers with 128 and 2 units respectively (see Fig. 4). Additionally, the final fully connected layer has a softmax activation function to express our class weights as a probability distribution. One advantage of ResNet 18 is that it has been pre-trained on the ImageNet data set which consists of over 1 million images divided into one thousand categories. Since the pre-training data set is so diverse, the ResNet model already has some general 'knowledge' of what it means for two images to be different. As a result, adapting ResNet to a new classification task should require fewer training examples than building a model from scratch. This is incredibly convenient given the amount of labor and time required to collect and label our training data.

At a high level, each convolution layer is essentially sliding some filter over the image with the idea that only relevant information makes it through the filter. We can imagine each image as a three dimensional tensor where the length of the last dimension is three, one for each color channel (RGB). The filter is then a four dimensional tensor, where each element along the first dimension represents a 3D tensor called a kernel. The values, or weights in each kernel are not necessarily equal, and in most cases should not be. In Fig. 3 we can see an example of a convolution operation with a filter size of 128, and kernels of size 3x3x3. The filter is aligned with the image (shaded in red) and we compute the Hadamard product between each kernel (orange) and the shaded region. We then sum the values in the resulting matrix and output. Thus, each kernel produces a single output, so each filter should produce a sequence of 128 outputs. In addition, we can see that one can only shift the filter 5 units in either direction without hitting a wall, so we expect a final output size of 5x5x128.

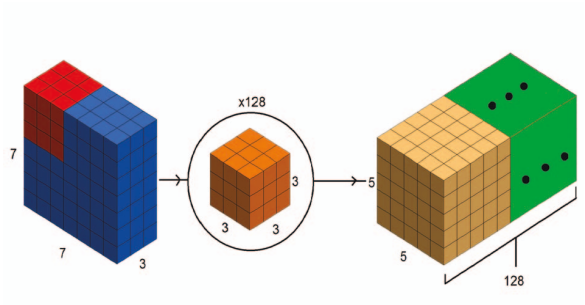

Fig. 3. A 2d convolution with 3 color channels, filter size of 128, and kernel size 3x3x3

During training, we will adjust the weights in each of the eighteen convolution layers and two fully connected layers according to the cross entropy loss function (Equation 1), specifically, the binary case when $M = 2$. Additionally we will employ stochastic gradient descent with momentum using learning rate = 0.001 and momentum = 0.9. After many training examples we expect the weights in each convolution layer to be learned such that the outputs of the final convolution are linearly separable with regard to their true class.

$$Cross\ Entropy = -\sum_{c=1}^{M} y_{o,c} \log(p_{o,c}) \tag{1}$$

where M is the number of classes, $y_{o,c}$ is a binary value equal to 1 if the observation's true class is the same as the class c otherwise 0, and $p_{o,c}$ is the predicted probability that the observation belongs to class c.

C. Image Preprocessing

Since ResNet only accepts images with red, green and blue color channels (RGB) of size 224x224 pixels with normalized channel values, we must transform our inputs to the correct shape and type. Each image is first resized to 256x256 pixels using bi-linear interpolation before being converted from gray scale to RGB with Floyd-Steinberg dithering. These transformed images can each be represented as a three dimensional tensor with shape (3, 256, 256) and real number values between 0 and 255. For training, we then perform a randomly centered square crop resulting in a final shape of (3, 224, 224). Additionally, during training each image has a 50% chance of being reflected about the y-axis. Each of these random operations serves to prevent the model from over fitting. Finally, the RGB values in each image tensor are standardized using the mean and standard deviation method (i.e. we subtract the mean from all pixel values and divide the result by the standard deviation for each color channel) with values derived from the ImageNet data set (see Table I).

TABLE I
MEAN AND STANDARD DEVIATIONS USED FOR NORMALIZATION GROUPED BY COLOR CHANNEL

Color Channel	R	G	B
Mean	.485	.456	.406
StdDev	.229	.224	.225

D. Evaluation Metrics

In the field of statistics and in particular for the purposes of prediction, four key terms are usually computed for assessing the performance of a classifier: true positives (tp), true negatives (tn), false positives (fp), and false negatives (fn). The terms positive and negative refer to the classifier's predicted label, and the terms true and false refer to whether that prediction corresponds to the external judgment, also known as the observation [23]. In our case, we will label any sample which exhibits adipogenic and/or osteogenic differentiation as a member of the positive class, while labelling all control samples as members of the negative class.

Some major measurement metrics: accuracy, precision, recall, F1 Score, and AUC are used to assess how well a binary classification is performed [23].

E. Imaging

Images were captured using the ZOE Fluorescent Cell Imager with an integrated digital camera (BIO-RAD). All fluorescence images were taken with the same setting for comparison. Data collection and imaging analysis were performed using NIH ImageJ software.

IV. RESULTS AND DISCUSSION

A. Experiments

We used an 80:20 split to divide the data set into 1,232 training images, and 301 validation images. Since the images are collected over the range of several days, our split is stratified such that equal proportions of images from each day are selected. That is, we take 80% of the 5 day images, 80% of the 7 day images, 80% of the 10 day images, and 80% of the 13 day images for our training set. The data set information is shown in Table II.

The model was trained for a total of twelve epochs with a batch size of 128. Throughout development we found that with this batch size, the model tended to converge on the training set between eight and twelve epochs. After training we selected the model with the greatest accuracy on the training data set in order to perform our validation and compute the discussed metrics.

TABLE II
DERMOSCOPIC DATA INFORMATION

Class	Days	Training Set	Test Set
Differentiation	5 days	245	60
	7 days	237	57
	10 days	239	58
	13 days	231	57
Control	5 days	80	20
	7 days	80	20
	10 days	40	10
	13 days	80	19
Total		1232	301

B. Results

Our model reached its maximum accuracy on the train data after eight epochs resulting in the performance metrics shown in Table III. We can see that the validation accuracy is exceptional with 97.34% of the images being correctly classified. Additionally, we can see in the confusion matrix (Figure 6) that the classification error is perfectly balanced between false positives and negatives meaning that $recall = precision = F1$. We can also observe from the AUC (Figure 5) that the model has a strong ability to distinguish between the positive and negative class, significantly outperforming random chance.

TABLE III
MODEL VALIDATION RESULTS

Metric	Value
Accuracy	0.9734
Precision	0.9828
Recall	0.9828
F1	0.9828
AUC	0.9873

Furthermore, if we assume that the classification error of our model is normally distributed, we can obtain a binomial confidence interval using a Wald interval. Given the fact that our model achieved a classification accuracy of 97.34% on a validation set of 301 images, we can therefore infer that the true accuracy of the model lies in the range [95.52%, 99.15%] with 95% confidence.

In "Morphology-Based Prediction of Osteogenic Differentiation Potential of Human Mesenchymal Stem Cells", Lan et al.

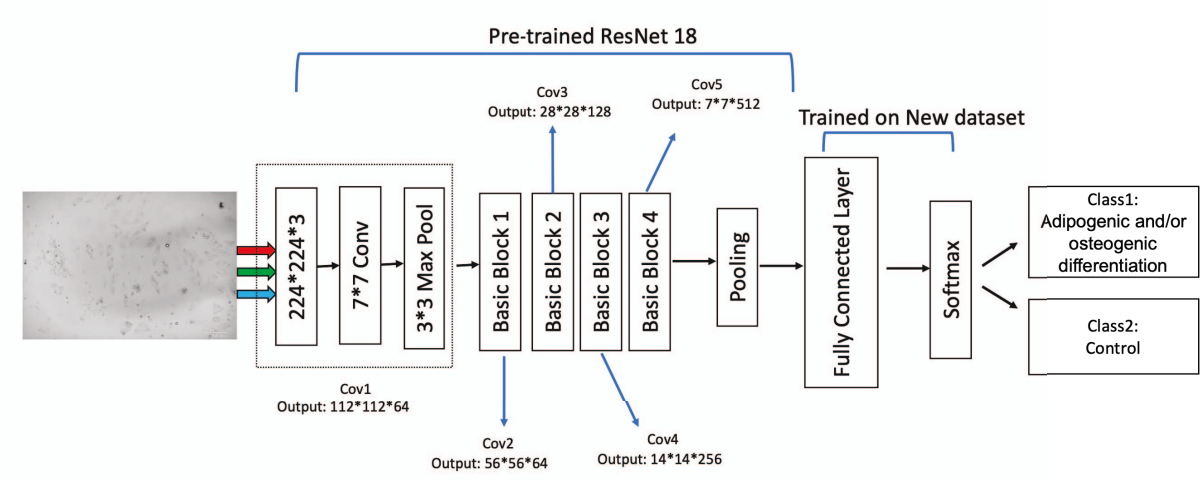

Fig. 4. Overview of ResNet 18 Models for Adipogenic Differentiation Identification

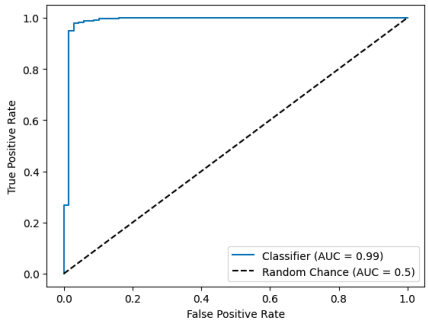

Fig. 5. AUC Curve

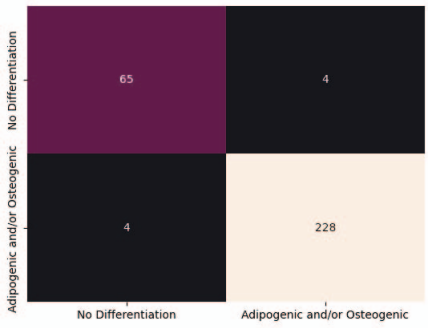

Fig. 6. Confusion Matrix

experimented using transfer learning with the Resnet50, InceptionV3, and VGG16 models for the purpose of classifying only differentiated osteocytes in a cell culture. In doing so they were able to obtain a, "high area under the curve (AUC) (0.94 ± 0.04)" [14] and "achieve(d) accuracy higher than 80% on the validation set except for day 0" [14]. Although Lan et al. were classifying only pure osteogenic differentiation as opposed to both adipogenic and osteogenic differentiation, it is still clear that our model was able to achieve a significantly greater level of performance as demonstrated by its greater accuracy and AUC. Additionally, our base model, Resnet18, has a total parameter count of approximately 11 million which is less than half that of both Resnet50 and InceptionV3 with around 26 and 27 million parameters respectively, and drastically smaller than VGG16 with 138 million parameters. As a result we are also able to retrain our model more quickly, perform faster predictions, and deploy the model to devices with limited hardware such as smartphones.

Since our training and validation data contains images taken at 5, 7, 10, and 13 days after sample collection, we also examined the performance of our model on each group via the same metrics. The reasoning for examining these groups is that although we are chemically inducing adipogenisis, not all cells begin the process at exactly the same time. As a result the proportion of differentiated cells increases as the culture ages. Additionally the process of adipogenisis can take up to two weeks before a cell is completely differentiated, meaning that over time cells will exhibit more of the morphological features of adipocytes. Our initial assumption was that images taken earlier in a culture's lifetime would be more difficult to identify. However, we can see from Table IV that the model was actually least accurate at the 13 day mark. In fact, there does not appear to be any strong relationship between the number of days since collection, and the model's accuracy. One explanation for this is that after 5 days the visual effects of adipogenic and osteogenic differentiation are already relatively pronounced. Additionally, after the 5 day mark we do not see any major changes in the defining visual characteristics of the differentiated cells, instead we tend to see them grow in number and size.

V. Conclusions and Future Work

In this study, we developed a deep learning-based algorithm using transfer learning on ResNet 18 to classify hMSCs adipogenic differentiation based on morphology changes. Our

TABLE IV
MODEL METRICS BY DAYS SINCE SAMPLE COLLECTION

Days	Accuracy	Precision	Recall	F1 Score	AUC
5 days	0.9750	0.9677	1.0000	0.9836	0.9642
7 days	0.9740	1.0000	0.9649	0.9821	1.0000
10 days	1.0000	1.0000	1.0000	1.0000	1.0000
13 days	.9474	0.9649	0.9649	0.9649	0.9917

model was able to attain an accuracy of 97.34%, AUC of 96.2%, and an F1 score of .9828 with a symmetric tradeoff between precision and recall. Furthermore, we were able to correctly classify images taken as early as 5 days after culturing with no appreciable drop in the models performance metrics. Therefore, this non-invasive approach, which only requires simple bright field microscope images, could be an effective aid in bio-manufacturing and research into cell-based therapies.

However, there are several avenues for future work that can extend and enhance our findings. Firstly, we will focus on identification and characterisation of the early differentiating cells (day 1, 2, 3 and 5). Additionally, we will apply the current state-of-the-art techniques and methodologies in cell segmentation to compute the proportion of differentiation for every image. These future directions will contribute to advancing the field of microscopy image recognition and provide valuable insights for practical applications of deep learning across the field.

ACKNOWLEDGMENT

S. Wang would like to acknowledge the support from the NSF CMMI program (Award number: 2143151).

REFERENCES

[1] A. Augello and C. De Bari, "The regulation of differentiation in mesenchymal stem cells," *Human Gene Therapy*, vol. 21, no. 10, pp. 1226–1238, 2010.

[2] T. Zhou, Z. Yuan, J. Weng, D. Pei, X. Du, C. He, and P. Lai, "Challenges and advances in clinical applications of mesenchymal stromal cells," *Journal of Hematology Oncology*, vol. 14, no. 1, pp. 1–24, 2021.

[3] S. Singh, A. E. Carpenter, and A. Genovesio, "Increasing the content of high-content screening: an overview," *Journal of Biomolecular Screening*, vol. 19, no. 5, pp. 640–650, 2014.

[4] C. Nombela-Arrieta, J. Ritz, and L. E. Silberstein, "The elusive nature and function of mesenchymal stem cells," *Nature Reviews Molecular Cell Biology*, vol. 12, no. 2, pp. 126–131, 2011.

[5] G. Kim, J. H. Jeon, K. Park, S. W. Kim, D. H. Kim, and S. Lee, "High throughput screening of mesenchymal stem cell lines using deep learning," *Scientific Reports*, vol. 12, no. 1, p. 17507, 2022.

[6] Y. Lan, N. Huang, Y. Fu, K. Liu, H. Zhang, Y. Li, and S. Yang, "Morphology-based deep learning approach for predicting osteogenic differentiation," *Frontiers in Bioengineering and Biotechnology*, vol. 9, p. 1521, 2022.

[7] F. Matsuoka, I. Takeuchi, H. Agata, H. Kagami, H. Shiono, Y. Kiyota, H. Honda, and R. Kato, "Morphology-based prediction of osteogenic differentiation potential of human mesenchymal stem cells," *PloS One*, vol. 8, no. 2, p. e55082, 2013.

[8] ——, "Characterization of time-course morphological features for efficient prediction of osteogenic potential in human mesenchymal stem cells," *Biotechnology and Bioengineering*, vol. 111, no. 7, pp. 1430–1439, 2014.

[9] J. Lo Surdo and S. R. Bauer, "Quantitative approaches to detect donor and passage differences in adipogenic potential and clonogenicity in human bone marrow-derived mesenchymal stem cells," *Tissue Engineering Part C: Methods*, vol. 18, no. 11, pp. 877–889, 2012.

[10] Y. Zhu, R. Huang, Z. Wu, S. Song, L. Cheng, and R. Zhu, "Deep learning-based predictive identification of neural stem cell differentiation," *Nature Communications*, vol. 12, no. 1, p. 2614, 2021.

[11] K. Fan, S. Zhang, Y. Zhang, J. Lu, M. Holcombe, and X. Zhang, "A machine learning assisted, label-free, non-invasive approach for somatic reprogramming in induced pluripotent stem cell colony formation detection and prediction," *Scientific Reports*, vol. 7, no. 1, p. 13496, 2017.

[12] M. Ashraf, M. Khalilitousi, and Z. Laksman, "Applying machine learning to stem cell culture and differentiation," *Current Protocols*, vol. 1, no. 9, p. e261, 2021.

[13] E. Ren, S. Kim, S. Mohamad, S. F. Huguet, Y. Shi, A. R. Cohen, E. Piddini, and R. C. Salas, "Deep learning-enhanced morphological profiling predicts cell fate dynamics in real-time in hpscs," *BioRxiv*, p. 2021.07. 31.454574, 2021.

[14] F. Matsuoka, I. Takeuchi, H. Agata, H. Kagami, H. Shiono, Y. Kiyota, H. Honda, and R. Kato, "Morphology-based prediction of osteogenic differentiation potential of human mesenchymal stem cells," *PloS one*, vol. 8, no. 2, p. e55082, 2013.

[15] D. Chen, S. Sarkar, J. Candia, S. J. Florczyk, S. Bodhak, M. K. Driscoll, C. G. Simon Jr, J. P. Dunkers, and W. Losert, "Machine learning based methodology to identify cell shape phenotypes associated with microenvironmental cues," *Biomaterials*, vol. 104, pp. 104–118, 2016.

[16] D. Chen, J. P. Dunkers, W. Losert, and S. Sarkar, "Early time-point cell morphology classifiers successfully predict human bone marrow stromal cell differentiation modulated by fiber density in nanofiber scaffolds," *Biomaterials*, vol. 274, p. 120812, 2021.

[17] H. Kim, K. Park, J.-M. Yon, S. W. Kim, S. Y. Lee, I. Jeong, J. Jang, S. Lee, and D.-W. Cho, "Predicting multipotency of human adult stem cells derived from various donors through deep learning," *Scientific Reports*, vol. 12, no. 1, p. 21614, 2022.

[18] Y. Zhou, X. Ping, Y. Guo, B. C. Heng, Y. Wang, Y. Meng, S. Jiang, Y. Wei, B. Lai, X. Zhang *et al.*, "Assessing biomaterial-induced stem cell lineage fate by machine learning-based artificial intelligence," *Advanced Materials*, p. 2210637, 2023.

[19] K. You, M. Long, Z. Cao, J. Wang, and M. I. Jordan, "Universal domain adaptation," in *Proceedings of the IEEE Conference on Computer Vision and Pattern Recognition*, 2019, pp. 2720–2729.

[20] A. Paszke, S. Gross, F. Massa, A. Lerer, J. Bradbury, G. Chanan, T. Killeen, Z. Lin, N. Gimelshein, L. Antiga *et al.*, "Pytorch: An imperative style, high-performance deep learning library," *Advances in Neural Information Processing Systems*, vol. 32, 2019.

[21] K. He, X. Zhang, S. Ren, and J. Sun, "Deep residual learning for image recognition," in *Proceedings of the IEEE Conference on Computer Vision and Pattern Recognition*, 2016, pp. 770–778.

[22] S. Guo and Z. Yang, "Multi-channel-resnet: An integration framework towards skin lesion analysis," *Informatics in Medicine Unlocked*, vol. 12, pp. 67–74, 2018.

[23] D. Olson and D. Delen, *Advanced Data Mining Techniques*. Springer Verlag, 2008.